

Variational simulation of d -level systems on qubit-based quantum simulators

Chufan Lyu,^{1,2} Zuoheng Zou,³ Xusheng Xu,³ Man-Hong Yung,^{3,4,5,6,7} and Abolfazl Bayat^{1,2,*}

¹*Institute of Fundamental and Frontier Sciences, University of Electronic Science and Technology of China, Chengdu 611731, China*

²*Key Laboratory of Quantum Physics and Photonic Quantum Information, Ministry of Education, University of Electronic Science and Technology of China, Chengdu 611731, China*

³*Central Research Institute, Huawei Technologies, Shenzhen, 518129, China*

⁴*Shenzhen Institute for Quantum Science and Engineering, Southern University of Science and Technology, Shenzhen, 518055, China*

⁵*International Quantum Academy, Shenzhen, 518048, China*

⁶*Guangdong Provincial Key Laboratory of Quantum Science and Engineering, Southern University of Science and Technology, Shenzhen, 518055, China*

⁷*Shenzhen Key Laboratory of Quantum Science and Engineering, Southern University of Science and Technology, Shenzhen, 518055, China*

Current quantum simulators are primarily qubit-based, making them naturally suitable for simulating 2-level quantum systems. However, many systems in nature are inherently d -level, including higher spins, bosons, vibrational modes, and itinerant electrons. To simulate d -level systems on qubit-based quantum simulators, an encoding method is required to map the d -level system onto a qubit basis. Such mapping may introduce illegitimate states in the Hilbert space which makes the simulation more sophisticated. In this paper, we develop a systematic method to address the illegitimate states. In addition, we compare two different mappings, namely binary and symmetry encoding methods, and compare their performance through variational simulation of the ground state and time evolution of various many-body systems. While binary encoding is very efficient with respect to the number of qubits it cannot easily incorporate the symmetries of the original Hamiltonian in its circuit design. On the other hand, the symmetry encoding facilitates the implementation of symmetries in the circuit design, though it comes with an overhead for the number of qubits. Our analysis shows that the symmetry encoding significantly outperforms the binary encoding, despite requiring extra qubits. Their advantage is indicated by requiring fewer two-qubit gates, converging faster, and being far more resilient to Barren plateaus. We have performed variational ground state simulations of spin-1, spin-3/2, and bosonic systems as well as variational time evolution of spin-1 systems. Our proposal can be implemented on existing quantum simulators and its potential is extendable to a broad class of physical models.

I. INTRODUCTION

The importance of quantum computation lies in their capability for exponential speedup in simulating quantum systems as well as addressing certain computational problems. Quantum computers are programmable machines that can implement any unitary operation on quantum systems and thus convert any quantum state in the Hilbert space to another. Any unitary operation can be decomposed into a combination of single-particle rotations as well as a two-particle entangling gate, the so-called universal gates. This creates the concept of digital quantum computation in which the design of a quantum computer reduces to implementation of the universal gates. Near-term noisy intermediate scale quantum (NISQ) devices, however, suffer from various imperfections, including limited connectivity, short coherence time, noisy gate operations, absence of quantum error correction, imperfect initialization, and faulty readout [1]. These imperfections make universal quantum computation inaccessible, at least, in a near future for

NISQ devices. Nonetheless, quantum simulators which are programmable machines with the capability of realizing a limited class of unitary operations for emulating complex quantum systems are feasible [2, 3]. Thanks to recent advancement in quantum technologies quantum simulators are emerging in various physical platforms, including optical lattices [4–6], Rydberg atoms [7, 8], optical chips [9–11], solid state systems [12], ion-traps [13–16], and superconducting devices [17–25]. These implementations are mostly qubit-based, making them naturally suitable for simulating two-level quantum systems.

Many systems in nature are inherently d -level (with $d > 2$), including higher spins [26], bosons [27], vibrational modes [28], and itinerant electrons [29]. In addition, there are classical optimization problems which can efficiently mapped to qudit systems [30, 31]. In principle, there are two methods for simulating such systems on quantum simulators. First, one can design and build d -level quantum simulators which can directly emulate those systems [32–40]. Second, one can rely on existing qubit-based quantum simulators but exploit proper encoding to effectively reproduce the behavior of d -level systems. The former approach is still technologically challenging and qudit quantum gates have only been considered for $d=3$ and $d=4$ with several practical difficul-

* abolfazl.bayat@uestc.edu.cn

ties [32–38]. The latter approach requires suitable encoding methods to map d -level systems to qubits. In Refs. [41–45], several encoding methods have been introduced to map a d -level system onto a qubit system. In these methods, depending on the mapping algorithm, a single d -level system can be mapped to a different number of qubits. While the most efficient mapping requires $\lceil \log_2(d) \rceil$ qubits, the other may demand d qubits. Note that, the complexity does not solely depend on the mapping as the manipulation of the qubits might be easier for a less efficient encoding. Simulating d -level systems on qubit-based quantum simulators may face several challenges: (i) mapping d -level systems to qubit systems can enlarge the corresponding Hilbert space, implying that certain regions of the Hilbert space does not represent the original system; (ii) the resulting qubit Hamiltonian may include multi-body interactions, which complicates the quantum simulation; (iii) symmetries of the original Hamiltonian may take complex forms after mapping to the qubits.

While universal quantum computation is not achievable with NISQ simulators, one may wonder whether such quantum devices can provide any computational advantage over classical computers. Indeed, the advantage of NISQ simulators has been demonstrated in sampling problems [10, 46, 47]. However, sampling problems do not have practical applications. Hence, achieving practical advantage with NISQ simulators is still an open problem. Variational Quantum Algorithms (VQAs) are the most promising approach for achieving quantum advantage in NISQ era. VQAs have been developed for a range of applications, including quantum chemistry [15, 48–52], combinatorial optimization [30, 53–55], quantum machine learning [56–63], dynamical simulations in closed [64–68] and open [66, 69–72] systems, quantum sensing [73–79], and condensed matter physics [16, 80, 81]. Variational Quantum Eigensolver (VQE) is an important class of VQAs which tend to simulate the low-energy eigenstates of a given Hamiltonian [50, 82–87]. Exploiting the inherent symmetries of the Hamiltonian in the VQE protocol, either through tailored circuit design [81, 88–94] or by incorporating them into the cost function as penalty terms [95, 96], is extremely beneficial in simplifying the protocol. However, most of these symmetry exploiting methods have been focused on qubit systems. Mapping symmetries of d -level quantum systems into qubit quantum circuits remains unexplored.

In this paper, we focus on the variational simulation of d -level systems on qubit-based quantum simulators. We first show that mapping from d -level systems to qubits may result in introduction of illegitimate states in the qubit Hilbert space which have no correspondence in the original system. We provide a systematic penalty approach to prevent these states to spoil our variational simulations. We then consider two different mappings, namely binary and symmetry encoding methods. Binary encoding is efficient with respect to the number of

qubits, though, it cannot incorporate symmetries in the circuit design. The symmetry encoding provides a natural way for incorporating the symmetries of the original Hamiltonian into the circuit of the qubit-based quantum simulators, although with an overhead of requiring extra qubits. Through comprehensive variational quantum simulation of the ground state and non-equilibrium dynamics of several spin and bosonic many-body systems, we demonstrate that symmetry encoding outperforms the binary mapping. This advantage reveals itself in fewer two-qubit gates, faster convergence, and less sensitivity to training issues such as Barren plateaus. Our proposal offers a promising and timely approach for simulating d -level systems on qubit-based platforms, with potential applications extendable to other types of quantum simulators.

II. VARIATIONAL QUANTUM ALGORITHMS

Variational Quantum Algorithms (VQAs) have emerged as a promising class of algorithms that leverage the hybrid quantum-classical approach to solve optimization problems and simulate quantum systems, particularly beneficial in the Noisy Intermediate-Scale Quantum (NISQ) era. In this section, we provide a brief introduction to the VQAs, focusing on their applications in preparing the ground state of a given Hamiltonian, or simulating non-equilibrium dynamics using the shallowest possible quantum circuit.

The Variational Quantum Eigensolver (VQE) is a pivotal example of VQA dedicated to finding the low energy eigenstates (e.g. the ground state) of a Hamiltonian, which is central to understanding the physical properties of quantum systems. In the VQE algorithm, a quantum state, denoted as $|\psi(\vec{\theta})\rangle$, is prepared through a parameterized quantum circuit acting on an initial state, expressed as $|\psi(\vec{\theta})\rangle = U(\vec{\theta})|\psi_0\rangle$, for a given N qubits. This parameterized quantum circuit, often referred as the ansatz, incorporates a set of tunable parameters $\vec{\theta} = (\theta_1, \theta_2, \dots, \theta_L)$, and $|\psi_0\rangle$ is the initial state. Varying $\vec{\theta}$ enables the output of the quantum circuit, namely $|\psi(\vec{\theta})\rangle$, to explore a segment of the Hilbert space, which is called reachable set. Notably, in circuits of significant depth, and thus a large number of parameters L , the reachable set can span the entire Hilbert space, allowing the preparation of any quantum state of N qubits. However, the goal is to keep the circuit as shallow as possible, focusing on the most relevant part of the Hilbert space. Specifically, VQE aims for a comparatively shallow ansatz that the reachable set contains the ground state of the Hamiltonian of interest H . Various ansatzes have been proposed, each differing in complexity [50, 97–101]. The expectation value of the Hamiltonian $\langle H \rangle = \langle \psi(\vec{\theta}) | H | \psi(\vec{\theta}) \rangle$ is measured at the output of the simulator. One then iteratively minimize $\langle H \rangle$ with respect to the parameters $\vec{\theta}$ using a classical optimization

algorithm, such as the gradient decent [102]. After a few iterations, $\langle H \rangle$ reaches its minimum for a special set of parameters $\vec{\theta}^*$. If the reachable set contains the ground state then the variational circuit with optimal parameters $\vec{\theta}^*$ produces the ground state of the Hamiltonian H .

The simulation of the ground state usually requires fewer resources than the non-equilibrium dynamics of many-body systems. This is because the entanglement in the ground state of local Hamiltonian is area-law while non-equilibrium states usually lead to the emergence of far more complex volume-law entangled states. Non-equilibrium dynamics of a quantum system is described by Schrödinger equation:

$$i \frac{d}{dt} |\psi(t)\rangle = H |\psi(t)\rangle. \quad (1)$$

The solution for a time-independent Hamiltonian is given by $|\psi(t)\rangle = e^{-iHt} |\psi_0\rangle$. There are two different methods to simulate non-equilibrium dynamics of a many-body system on a digital quantum simulator: (i) Trotterization of the unitary operation e^{-iHt} ; and (ii) variational simulation of the non-equilibrium dynamics. The former requires a deep quantum circuit to keep the Trotterization error below an acceptable range [81]. The latter is possibly more NISQ friendly as the use of a classical optimization may help to simplify the quantum circuit. In this paper, we focus on a variational algorithm, developed in Refs. [66, 103], for simulating non-equilibrium dynamics of d -level systems on qubit-based quantum computers. We employ a parameterized trial state $|\psi(\vec{\theta}(t))\rangle$ with time-dependent parameters $\vec{\theta}(t)$. For variational quantum simulation, the trial state is prepared by a variational quantum circuit $U(\vec{\theta}(t))$ acting on an initial state $|\psi_0\rangle$, e.g. $|\psi(\vec{\theta}(t))\rangle = U(\vec{\theta}(t)) |\psi_0\rangle$. Assuming the state at time t is obtained by $|\psi(t)\rangle = |\psi(\vec{\theta}(t))\rangle$, the goal is to approximate the state $|\psi(t + \delta t)\rangle$. According to the Schrödinger equation, the state evolves from time t to $t + \delta t$ as follows:

$$|\psi(t + \delta t)\rangle \approx |\psi(\vec{\theta}(t))\rangle - i\delta t H |\psi(\vec{\theta}(t))\rangle. \quad (2)$$

Given that the variational trial state $|\psi(\vec{\theta}(t + \delta t))\rangle$ is trying to find the optimal solution $\vec{\theta}(t + \delta t)$ that best approximates the state within its reachable set, we have:

$$|\psi(\vec{\theta}(t + \delta t))\rangle \approx |\psi(\vec{\theta}(t))\rangle - i\delta t H |\psi(\vec{\theta}(t))\rangle. \quad (3)$$

Note that, by focusing on the variation of the trial state with changing parameters, we have:

$$|\psi(\vec{\theta}(t + \delta t))\rangle \approx |\psi(\vec{\theta}(t))\rangle + \sum_j \frac{\partial |\psi(\vec{\theta}(t))\rangle}{\partial \theta_j} \delta \theta_j, \quad (4)$$

where $\delta \theta_j = \theta_j(t + \delta t) - \theta_j(t)$. The objective is then to find the optimal $\vec{\theta}(t + \delta t)$ that minimizes the difference between the evolved state according to the Schrödinger

equation and the variational approximation:

$$\sum_j \frac{\partial |\psi(\vec{\theta}(t))\rangle}{\partial \theta_j} \delta \theta_j \approx -i\delta t H |\psi(\vec{\theta}(t))\rangle. \quad (5)$$

Assuming the parameters are real, applying McLachlan's variational principle gives:

$$\sum_j A_{i,j}^R \dot{\theta}_j = C_i^I, \quad (6)$$

where A and \vec{C} are defined as:

$$A_{i,j} = \frac{\partial \langle \psi(\vec{\theta}(t)) |}{\partial \theta_i} \frac{\partial |\psi(\vec{\theta}(t))\rangle}{\partial \theta_j}, \quad (7)$$

$$C_i = \frac{\partial \langle \psi(\vec{\theta}(t)) |}{\partial \theta_i} H |\psi(\vec{\theta}(t))\rangle.$$

Here, $A_{i,j}^R$ and C_i^I represent the real and imaginary parts of $A_{i,j}$ and C_i , respectively. The derivatives of the time-dependent parameters, $\vec{\theta}$, are thus given by $\dot{\vec{\theta}} = A^{R-1} \vec{C}^I$. By updating the parameters as:

$$\vec{\theta}(t + \delta t) = \vec{\theta}(t) + \delta t A^{R-1} \vec{C}^I, \quad (8)$$

and repeating this process $T/\delta t$ times, the time evolution over a duration T is simulated. Fig. 1(e) illustrates the circuit implementation for evaluating the real and imaginary parts of the matrix A and vector C .

In the domain of VQAs, resource efficiency emerges as a critical property due to the constraints imposed by NISQ devices. These devices are typically characterized by a limited number of qubits, brief coherence times, and elevated error rates. As a result, a quantification of resource efficiency is essential for assessing the performance of VQAs. This efficiency can be dissected into two primary categories: classical and quantum resources. Classical resources primarily depend on the computational demands of the optimization process, notably the number of iterations needed to tune the parameters. Furthermore, each parameter requires individual measurements for gradient evaluation if the optimizer in the VQAs adopted to gradient-based optimizer. Thus, we define the measure of Classical Resources (C_R) as the product of the number of parameters L and the number of optimization iterations n_I , expressed mathematically as:

$$C_R = L \times n_I \quad (9)$$

For quantum resources, the emphasis is on the circuit components that are most susceptible to noises on NISQ devices. Since single-qubit operations are relatively error-resilient and precise, the focus shifts to two-qubit entangling operations, which are more prone to errors. Hence, we quantify quantum resources by the number of two-qubit entangling gates used in the circuit.

Therefore, in consideration of developing a VQA, selecting an appropriate ansatz is essential for achieving

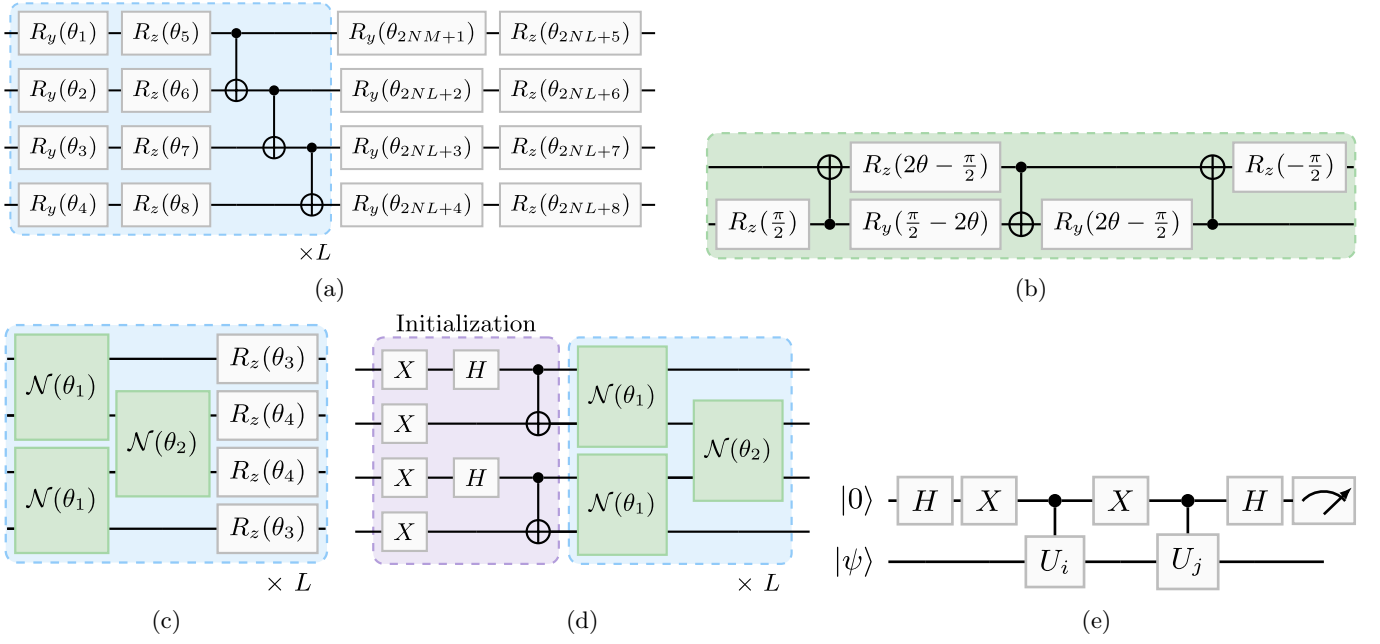


FIG. 1: (a) The hardware efficient ansatz circuit for system size $N=4$. The circuits highlighted in blue can be repeated to increase the expressibility of the variational circuit. (b) Circuit implementing of $\mathcal{N}(\theta_x, \theta_y, \theta_z)$ as an entangling gate between two qubits. (c) The s_z -conserving ansatz circuit for system size $N=4$. (d) The total spin conserving ansatz circuit for system size $N=4$. (e) Circuit implementation for evaluating the coefficients in a quantum simulator. The qubit on the top is an ancillary qubit. The probability of measuring the ancillary qubit in the state $|0\rangle$ is: $P_0 = \left(1 + \Re(\langle\psi|U_i^\dagger U_j|\psi\rangle)\right)/2$. One can utilize the same circuit with a phase gate $S = \begin{pmatrix} 1 & 0 \\ 0 & i \end{pmatrix}$ applied to the ancillary qubit before the last Hadamard gate to measure the imaginary part of the coefficient.

an optimal balance between minimizing the use of error-prone two-qubit gates and controlling the number of variational parameters. The former is crucial for quantum resource efficiency, and the latter not only dictates the expansiveness of the reachable set but also influences the efficiency of classical resources.

One of the most commonly used ansatzes in the literature is the hardware-efficient ansatz, depicted in Fig. 1(a). This ansatz consists of alternating layers of single-qubit rotations and two-qubit entangling gates. The single-qubit rotations are defined by the formula:

$$R_\alpha(\theta) = e^{-i\theta\sigma^\alpha/2}, \quad (10)$$

where σ^α is the Pauli operator, with $\alpha \in \{x, y, z\}$. For the two-qubit operations, we employ the Controlled-Not (CNOT) gate, which is specified by the matrix:

$$\text{CNOT} = \begin{pmatrix} 1 & 0 & 0 & 0 \\ 0 & 1 & 0 & 0 \\ 0 & 0 & 0 & 1 \\ 0 & 0 & 1 & 0 \end{pmatrix}. \quad (11)$$

This structure is particularly favored for its simplicity and efficiency in creating entanglement between qubits, which is critical for the success of various variational quantum algorithms. Nonetheless, the hardware-efficient ansatz suffers from Barren plateau [104, 105], which

makes its training challenging for large-scale quantum systems. Furthermore, this ansatz does not inherently preserve any symmetries that may exist in the Hamiltonian, which could enhance quantum simulation performance. As an alternative, one might consider a more complex entangling gate with tunable parameters, such as [106]:

$$\mathcal{N}(\theta_x, \theta_y, \theta_z) = e^{i(\theta_x \sigma^x \otimes \sigma^x + \theta_y \sigma^y \otimes \sigma^y + \theta_z \sigma^z \otimes \sigma^z)}, \quad (12)$$

where $\sigma^x \otimes \sigma^x$, $\sigma^y \otimes \sigma^y$, and $\sigma^z \otimes \sigma^z$ are the tensor products of the Pauli operators acting on two qubits. The circuit implementation of this unitary operation is depicted in Fig. 1(b). In the special case where $\theta_x = \theta_y = \theta_z = \theta$, this unitary conserves the number of excitations as well as the total spin. By combining this entangling gate with single-qubit rotations, for example $R_z(\theta)$, one can construct an excitation preserving ansatz, $U(\vec{\theta})$, satisfying $[U(\vec{\theta}), S_{tot}^z] = 0$, where $S_{tot}^\alpha = \frac{1}{2} \sum_i \sigma_i^\alpha$ for $\alpha \in \{x, y, z\}$, as illustrated in Figs. 1(c). In the absence of single-qubit rotations on the z -axis, namely $R_z(\theta)$, the ansatz preserves the total spin, i.e. $[U(\vec{\theta}), S_{tot}^2] = 0$, where $S_{tot}^2 = (S_{tot}^x)^2 + (S_{tot}^y)^2 + (S_{tot}^z)^2$, shown in Fig. 1(d).

III. QUDIT TO QUBIT MAPPING

The first step towards the simulation of a d -level many-body quantum system on a qubit-based quantum simulator is to exploit an encoding algorithm which maps the d -level operators into qubit operators. Several encoding techniques have been explored [41–44]. The most straightforward method is the binary encoding in which a d -level particle is mapped to $M = \lceil \log_2(d) \rceil$ qubits, where $\lceil x \rceil$ represents the smallest integer number that is greater or equal to the real number x . In this encoding, each d -level basis state $|\tilde{j}\rangle$ ($j = 0, 1, \dots, d-1$) is mapped to the binary representation of its index j , which is converted into an M -qubit computational state. The binary representation is padded with zeros on the left to match the number of qubits n :

$$|\tilde{j}\rangle \mapsto |\mathbf{b}_M^{(j)}\rangle = |b_{M-1}b_{M-2}\dots b_1b_0\rangle \quad (13)$$

where $b_{M-1}b_{M-2}\dots b_1b_0$ is the binary representation of the integer j padded to M bits. For instance, for a 9-level qudit system, we require 4 qubits to encode $|\tilde{0}\rangle = |0000\rangle$ all the way to $|\tilde{8}\rangle = |1000\rangle$. Note that throughout this paper the tilde basis $|\tilde{j}\rangle$ is used for qudits and the ordinary basis $|j\rangle$ is used for qubits. It will be convenient to define the transformation operator between the two bases as

$$\mathcal{T}_b = \sum_{j=0}^{d-1} |\mathbf{b}_M^{(j)}\rangle \langle \tilde{j}|. \quad (14)$$

Note that while we always have $\mathcal{T}_b^\dagger \mathcal{T}_b = \mathbb{I}_{\text{qudits}}$, the vice versa is not always valid, i.e. $\mathcal{T}_b \mathcal{T}_b^\dagger \neq \mathbb{I}_{\text{qubits}}$, unless $M = \log_2(d)$. By using the transformation matrix \mathcal{T}_b , one can map any qudit operator \tilde{H} into a qubit basis through $H = \mathcal{T}_b \tilde{H} \mathcal{T}_b^\dagger$ and then write it in terms of Pauli strings with the help of the following maps:

$$\begin{aligned} |0\rangle\langle 0| &= \frac{1}{2}(\mathbb{I} + \sigma^z), & |1\rangle\langle 1| &= \frac{1}{2}(\mathbb{I} - \sigma^z), \\ |0\rangle\langle 1| &= \frac{1}{2}(\sigma^x + i\sigma^y), & |1\rangle\langle 0| &= \frac{1}{2}(\sigma^x - i\sigma^y), \end{aligned} \quad (15)$$

where \mathbb{I} is the identity and $\sigma^{x,y,z}$ are the Pauli operators.

If the qudit Hamiltonian \tilde{H} supports a symmetry \tilde{S} , namely $[\tilde{H}, \tilde{S}] = 0$, the corresponding qubit Hamiltonian $H = \mathcal{T}_b \tilde{H} \mathcal{T}_b^\dagger$ supports an equivalent symmetry $S = \mathcal{T}_b \tilde{S} \mathcal{T}_b^\dagger$. However, even if \tilde{S} might be a simple local operator the form of S might be complex consisting of several multi-qubit terms in the qubit basis. It has been shown that in VQE simulations, the most resource efficient approach to benefit from the symmetries is to incorporate them in the design of the circuit such that $[U(\tilde{\theta}), S] = 0$ [97]. In this situation, the circuit preserves the symmetries in the initial state and thus makes the VQE simulation easier. The problem is that if the symmetry operator S is complex itself then designing such

a circuit becomes challenging. This is often the case for mapping qudits to qubits. Therefore, an alternative mapping might be exploited, namely symmetry encoding. This approach maps each d -level basis state $|\tilde{j}\rangle$ into a superposition of $d-1$ computational qubit states with exactly j excitations:

$$|\tilde{j}\rangle \mapsto |\mathbf{f}_{d-1}^{(j)}\rangle = \frac{1}{\sqrt{\binom{d-1}{j}}} \sum_{\substack{\forall k \text{ with } j \\ \text{excitations}}} |\mathbf{b}_{d-1}^{(k)}\rangle \quad (16)$$

where $\binom{d-1}{j}$ is the binomial coefficient which guarantees the normalization, $|\mathbf{b}_{d-1}^{(k)}\rangle$ is given in Eq. (13) and summation runs over all values of $k = 0, \dots, d-1$ in which $|\mathbf{b}_{d-1}^{(k)}\rangle$ has only j excitations. One can define the transformation operator between the two bases as

$$\mathcal{T}_s = \sum_{j=0}^{d-1} |\mathbf{f}_{d-1}^{(j)}\rangle \langle \tilde{j}|. \quad (17)$$

The symmetry encoding scheme effectively preserves certain types of symmetries, for example the conservation of components of the total spin in a spin system, i.e. $[\tilde{H}, \tilde{S}_{tot}^\alpha] = [H, S_{tot}^\alpha] = 0$, where $\tilde{S}_{tot}^\alpha = \frac{1}{2} \sum_i \tilde{S}_i^\alpha$, ($\alpha = x, y, z$) (Similar definition is given for S_{tot}^α in the qubit basis). Here, \tilde{S}_i^α is the α -component of the spin operator acting on the i -th site of the d -level system. This conservation implies that the symmetry-preserving encoding also preserves the conservation of total spin from d -level to qubit systems, i.e. $[\tilde{H}, \tilde{S}_{tot}^2] = [H, S_{tot}^2] = 0$, where $\tilde{S}_{tot}^2 = (\tilde{S}_{tot}^x)^2 + (\tilde{S}_{tot}^y)^2 + (\tilde{S}_{tot}^z)^2$ (again similar definition is valid for S_{tot}^2 in the qubit basis).

Although, in general, using the symmetry encoding demands extra qubits than the binary one, it allows one to use ansatzes which have been developed for preserving certain symmetries such as total spin or number of excitations [91, 97]. Those ansatzes are way more resource efficient for variational simulation than the conventional hardware efficient ansatz which does not preserve symmetries. Therefore, the final performance of the symmetric encoding in comparison with the binary encoding relies on two opposite factors, namely the use of extra qubits for the encoding versus the access to more resource efficient circuits. Determining which of these factors is going to play a more important role in variational simulation of d -level systems is the subject of this paper.

It is important to note that, for both of the encoding methods, the Hilbert space of the qubit system is larger than (or at least equal to) the one for the qudit system. For instance, in a many-body system of N qudit particles the size of the Hilbert space is d^N . While using the binary encoding enlarges the size of the Hilbert space to 2^{NM} and using symmetry encoding enlarges it even more to $2^{N(d-1)}$. As a result, certain states within the encoded qubit system are “illegitimate”, i.e. having no counterpart in the qudit system. Thus, for any quantum state $|\phi\rangle$ within the illegitimate subspace one inherently gets

$H|\phi\rangle = 0$. The illegitimate states can indeed complicate the simulation process, particularly in VQE implementations, where such states may erroneously appear as the state with minimum energy. This issue typically arises when the actual ground state of the d -level system has an average energy greater than zero, namely $\langle \tilde{g}\tilde{s}|\tilde{H}|\tilde{g}\tilde{s}\rangle > 0$. Under these conditions, the illegitimate states, which inherently possess zero energy, will be the ground state of the encoded qubit system. To address this issue, one can incorporate a penalty term into the cost function of the VQE that specifically pushes the energy of these states upward.

To exemplify the inclusion of penalty term, consider a symmetry encoding on a spin-1 system with 3-level basis states

$$|\tilde{0}\rangle = |s_z = +1\rangle, \quad |\tilde{1}\rangle = |s_z = 0\rangle, \quad |\tilde{2}\rangle = |s_z = -1\rangle, \quad (18)$$

where $|s_z\rangle$ represents the z -component of the spin-1 particles. The symmetry encoding results in

$$|\tilde{0}\rangle \mapsto |00\rangle, \quad |\tilde{1}\rangle \mapsto \frac{1}{\sqrt{2}}(|01\rangle + |10\rangle), \quad |\tilde{2}\rangle \mapsto |11\rangle. \quad (19)$$

In this mapping, the singlet state $\frac{1}{\sqrt{2}}(|01\rangle - |10\rangle)$ is not used and thus considered as illegitimate. To effectively penalize this state, the following penalty term is naturally constructed for the neighboring pairs of qubits which encode one spin-1 particle:

$$\begin{aligned} \mathcal{P}_{i,i+1} = & |00\rangle\langle 00| + \frac{1}{2}(|01\rangle + |10\rangle)(\langle 01| + \langle 10|) \\ & + |11\rangle\langle 11| - \frac{1}{2}(|01\rangle - |10\rangle)(\langle 01| - \langle 10|). \end{aligned} \quad (20)$$

By considering the Eq. (15) one can simplify this penalty term into:

$$\mathcal{P}_{i,i+1} = -(\sigma_i^x \otimes \sigma_{i+1}^x + \sigma_i^y \otimes \sigma_{i+1}^y + \sigma_i^z \otimes \sigma_{i+1}^z). \quad (21)$$

So, the cost function of the VQE will be updated to

$$\text{cost} = \langle H \rangle + \beta \sum_{\text{odd } i} \langle \mathcal{P}_{i,i+1} \rangle, \quad (22)$$

where β is a sufficiently large positive scalar. By minimizing this updated cost function the VQE naturally penalizes the illegitimate states energetically and ensures that the output state of the qubit-based simulator accurately reflects the ground state of the d -level system.

IV. VARIATIONAL GROUND STATE SIMULATION

In this section, we present the VQE algorithm for simulating the ground state of d -level systems using qubit-based quantum simulators.

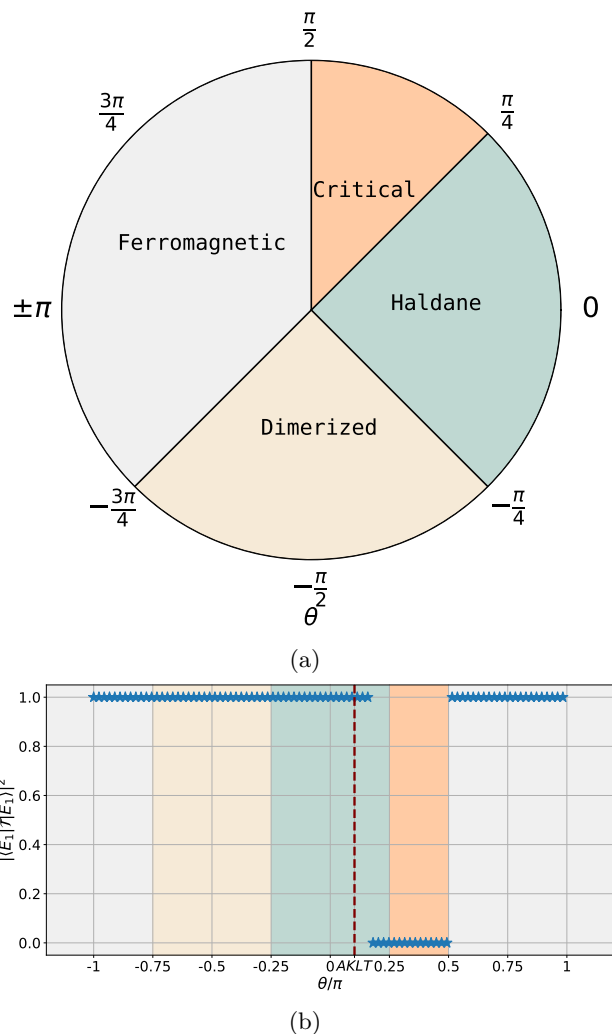


FIG. 2: (a) The phase diagram of the spin-1 bilinear biquadratic Heisenberg model. (b) The fidelity between the true qudit ground state $|\tilde{E}_1\rangle$ of the spin-1 BBH model with a system size of $N=6$ and the ground state of the encoded 12-qubit Hamiltonian $|E_1\rangle$ across the phase diagram, namely $|\langle E_1 | \mathcal{T} | \tilde{E}_1 \rangle|^2$. Note that the result is valid for both binary and symmetry encoding methods.

A. VQE simulation of spin-1 models

Specifically, we first focus on the simulation of a spin-1 system (i.e. $d=3$). We consider the Bilinear-Biquadratic Heisenberg (BBH) model of size N , defined as:

$$\tilde{H}_{\text{BBH}} = J \sum_{i=1}^{N-1} \left[\cos(\theta) \tilde{S}_i \cdot \tilde{S}_{i+1} + \sin(\theta) (\tilde{S}_i \cdot \tilde{S}_{i+1})^2 \right], \quad (23)$$

where J is the coupling strength. In our ground state simulation, we put $J=1$. $\tilde{S}_i = (\tilde{S}_i^x, \tilde{S}_i^y, \tilde{S}_i^z)$ represents the spin-1 operators at the i -th site, with matrices given

by:

$$\begin{aligned}\tilde{S}^x &= \frac{1}{\sqrt{2}} \begin{pmatrix} 0 & 1 & 0 \\ 1 & 0 & 1 \\ 0 & 1 & 0 \end{pmatrix} \\ \tilde{S}^y &= \frac{1}{\sqrt{2}} \begin{pmatrix} 0 & -i & 0 \\ i & 0 & -i \\ 0 & i & 0 \end{pmatrix} \\ \tilde{S}^z &= \begin{pmatrix} 1 & 0 & 0 \\ 0 & 0 & 0 \\ 0 & 0 & -1 \end{pmatrix}.\end{aligned}\quad (24)$$

The BBH model is a generalization of the Heisenberg model that includes both bilinear and biquadratic interactions between neighboring spins. The parameter θ controls the relative strength of these interactions. The spin-1 BBH model exhibits several symmetries, including the conservation of the total spin, expressed as $[\tilde{H}_{\text{BBH}}, \tilde{S}_{\text{tot}}^2] = 0$. This conservation law implies that every eigenstate $|\tilde{E}_k\rangle$ of the BBH model possesses a well-defined total spin s , which is an integer for even system sizes N and a half-integer for odd N . Consequently, the expectation value of the total spin operator for any eigenstate is given by $\langle \tilde{E}_k | \tilde{S}_{\text{tot}}^2 | \tilde{E}_k \rangle = s(s+1)$. Additionally, the conservation of total spin implies the conservation of its components in all directions, i.e., $[\tilde{H}_{\text{BBH}}, \tilde{S}_{\text{tot}}^\alpha] = 0$, which ensures that the z -component of the total spin, \tilde{S}_{tot}^z , for each eigenstate is also conserved such that $\langle \tilde{E}_k | \tilde{S}_{\text{tot}}^z | \tilde{E}_k \rangle = s_z$, with s_z ranging from $-s$ to s .

The spin-1 BBH model is well-known in condensed matter physics for exhibiting a rich phase diagram as θ varies from $-\pi$ to π . The schematic of the phase diagram is shown in Fig. 2(a). In the range $\theta \in [-\frac{3}{4}\pi, \frac{1}{2}\pi]$ the system is in a ferromagnetic phase, where all spins are aligned in the same direction, making the ground state trivial to simulate. We therefore focus our VQE simulations on the non-trivial phases of the BBH model. For $\theta \in [-\frac{3}{4}\pi, -\frac{1}{4}\pi]$, the system is in the dimerized phase with broken translational invariance and singlets of neighboring spins. The ground state in this phase transition can be characterized by the order parameter [107]:

$$\mathcal{O}_{\text{dimer}} = |\langle H_i - H_{i+1} \rangle|,$$

where $H_i = \cos(\theta) \tilde{S}_i \cdot \tilde{S}_{i+1} + \sin(\theta) (\tilde{S}_i \cdot \tilde{S}_{i+1})^2$. In large systems or periodic boundary conditions, the choice of index i does not matter. Nonetheless, in finite open systems we select $i = 2$ to avoid being at the boundary. Notably, for $\theta \in [-\frac{1}{4}\pi, \frac{1}{4}\pi]$, the system is in the Haldane phase, which is a topological phase. Particularly, at the $\theta = \arctan(1/3)$ point, known as the Affleck-Kennedy-Lieb-Tasaki (AKLT) point, the ground state is four-fold degenerate, including a singlet state with total spin $s = 0$ and a triplet state with total spin $s = 1$. The Haldane topological phase can be characterized by a string order

parameter [107]:

$$\mathcal{O}_{\text{Haldane}} = \lim_{r \rightarrow \infty} \left\langle S_i^z \exp \left[i\pi \sum_{j=i+1}^{i+r-1} S_j^z \right] S_{i+r}^z \right\rangle, \quad (25)$$

with r being the size of the string. Although, ideally r has to be large in our finite system it will be a finite number. In the region where $\theta \in [\frac{1}{4}\pi, \frac{1}{2}\pi]$, the ground state is in the critical phase, which is a gapless phase. The existence of this phase can be reflected by a nematic structure factor at $q = 2\pi/3$, which is defined as [107]

$$S(q) = \frac{1}{N} \sum_{k,l} e^{iq(k-l)} \langle (S_k^z)^2 (S_l^z)^2 \rangle.$$

The first step towards the VQE simulation of the Hamiltonian (23) is to generate its qubit representation. Interestingly, for spin-1 systems both binary and symmetry encodings demand exactly 2 qubits for representing each spin. This provides an opportunity to compare the performance of these two encodings using the same number of qubits. In order to map the Hamiltonian into a qubit basis one has to use the transformation $H = \mathcal{T}^{\otimes N} \tilde{H} \mathcal{T}^{\dagger \otimes N}$, where \mathcal{T} stands for \mathcal{T}_b (for binary encoding) and \mathcal{T}_s for symmetric encoding. Note that one has to pay extra attention to this transformation, in particular, when illegitimate states are also involved. This is because $\mathcal{T} \mathcal{T}^\dagger \neq \mathbb{I}_{\text{qubit}}$. Consequently, the transformation has to apply to the interaction terms $\tilde{S}_i \cdot \tilde{S}_{i+1}$ and $(\tilde{S}_i \cdot \tilde{S}_{i+1})^2$, rather than directly on the spin-1 operators \tilde{S}^α (with $\alpha = x, y, z$) and then use tensor product. The exact form of the transformation for the symmetric encoding is in the following (for the binary transformation, please see appendix A)

$$\begin{aligned}\tilde{S}_i \cdot \tilde{S}_{i+1} &\mapsto \frac{1}{4} \left(\sigma_{j+1}^x \sigma_{j+3}^x + \sigma_{j+1}^x \sigma_{j+2}^x \right. \\ &\quad + \sigma_j^x \sigma_{j+3}^x + \sigma_j^x \sigma_{j+2}^x + \sigma_{j+1}^y \sigma_{j+3}^y + \sigma_{j+1}^y \sigma_{j+2}^y \\ &\quad + \sigma_j^y \sigma_{j+3}^y + \sigma_j^y \sigma_{j+2}^y + \sigma_j^z \sigma_{j+2}^z + \sigma_j^z \sigma_{j+3}^z \\ &\quad \left. + \sigma_{j+1}^z \sigma_{j+2}^z + \sigma_{j+1}^z \sigma_{j+3}^z \right)\end{aligned}\quad (26)$$

$$\begin{aligned}
(\vec{S}_i \cdot \vec{S}_{i+1})^2 &\mapsto \frac{3}{4}I + \frac{1}{4} \left(\sigma_{j+2}^x \sigma_{j+3}^x \right. \\
&+ \sigma_j^x \sigma_{j+1}^x + \sigma_j^x \sigma_{j+1}^x \sigma_{j+2}^x \sigma_{j+3}^x \left. \right) \\
&- \frac{1}{8} \left(\sigma_{j+1}^z \sigma_{j+3}^z + \sigma_{j+1}^y \sigma_{j+3}^y + \sigma_{j+1}^z \sigma_{j+2}^z \right. \\
&+ \sigma_{j+1}^y \sigma_{j+2}^y + \sigma_j^z \sigma_{j+3}^z + \sigma_j^y \sigma_{j+3}^y \\
&+ \sigma_j^z \sigma_{j+2}^z + \sigma_j^y \sigma_{j+2}^y + \sigma_{j+1}^x \sigma_{j+3}^x \\
&+ \sigma_{j+1}^x \sigma_{j+2}^x + \sigma_j^x \sigma_{j+3}^x + \sigma_j^x \sigma_{j+2}^x \left. \right) \\
&+ \frac{1}{8} \left(\sigma_j^y \sigma_{j+1}^x \sigma_{j+2}^x \sigma_{j+3}^x + \sigma_j^z \sigma_{j+1}^x \sigma_{j+2}^x \sigma_{j+3}^z \right. \\
&+ \sigma_j^y \sigma_{j+1}^x \sigma_{j+2}^y \sigma_{j+3}^z + \sigma_j^z \sigma_{j+1}^x \sigma_{j+2}^y \sigma_{j+3}^z \\
&+ \sigma_j^x \sigma_{j+1}^y \sigma_{j+2}^x \sigma_{j+3}^x + \sigma_j^x \sigma_{j+1}^z \sigma_{j+2}^x \sigma_{j+3}^x \\
&+ \sigma_j^x \sigma_{j+1}^y \sigma_{j+2}^y \sigma_{j+3}^z + \sigma_j^x \sigma_{j+1}^z \sigma_{j+2}^y \sigma_{j+3}^z \\
&+ \sigma_j^z \sigma_{j+1}^y \sigma_{j+2}^y \sigma_{j+3}^z + \sigma_j^z \sigma_{j+1}^y \sigma_{j+2}^z \sigma_{j+3}^z \\
&+ \sigma_j^y \sigma_{j+1}^z \sigma_{j+2}^y \sigma_{j+3}^z + \sigma_j^y \sigma_{j+1}^z \sigma_{j+2}^z \sigma_{j+3}^z \left. \right) \\
&+ \frac{1}{4} \left(\sigma_{j+2}^y \sigma_{j+3}^y + \sigma_j^y \sigma_{j+1}^y + \sigma_j^y \sigma_{j+1}^y \sigma_{j+2}^y \sigma_{j+3}^y \right. \\
&+ \sigma_{j+2}^z \sigma_{j+3}^z + \sigma_j^z \sigma_{j+1}^z + \sigma_j^z \sigma_{j+1}^z \sigma_{j+2}^z \sigma_{j+3}^z \left. \right) \quad (27)
\end{aligned}$$

where $j = 2i - 1$ represents the corresponding index of the spin-1 operator in the qubit system.

It is insightful to check whether the ground state of the qubit Hamiltonian $|E_1\rangle$ truly represents the true qubit ground state $|\tilde{E}_1\rangle$ through the fidelity $|\langle E_1 | \mathcal{T} | \tilde{E}_1 \rangle|^2$. In Fig. 2(b), we present the fidelity result $|\langle E_1 | \mathcal{T} | \tilde{E}_1 \rangle|^2$ for the spin-1 BBH model with a system size of $N=6$, which corresponds to a 12-qubit encoded Hamiltonian, across the phase diagram. Apparently, in the critical phase and part of the Haldane phase, this fidelity drops to zero showing that illegitimate states are indeed taking the low energy states. Note that, the result is valid for both binary and symmetry encoding methods. Therefore, without including penalty terms, see Eq. (22), one cannot target the true ground state.

In order to have a comparison between the binary and the symmetry encodings we focus on the VQE simulation of the ground state. In both cases to simulate a many-body system of size N , we need $2N$ qubits. We start with the simulation using the binary encoding method in which we use the hardware efficient circuit as the variational ansatz. The results of the VQE simulations for the BBH model with a system size of $N=6$, namely a 12 qubit system after applying binary encoding, are presented in Fig. 3. The average obtainable fidelity of the ground state with respect to the true ground state of the BBH model is plotted as a function of the optimization iterations for different values of θ . All the simulations in this paper use the gradient-based L-BFGS-B optimizer [102] for minimizing their cost function. The results are averaged over 50 independent runs. It is clear from the simulations that none of them has converged to the ground state of the BBH model with a fidelity $\mathcal{F} \geq 0.85$. Ad-

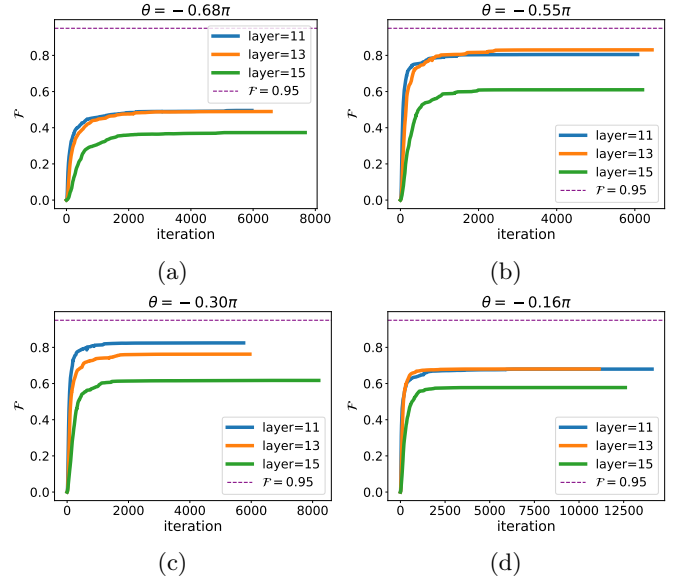


FIG. 3: The VQE simulation of the ground state of the spin-1 BBH model with system size $N=6$ for different values of θ . The corresponding qubit Hamiltonian uses 12 qubits, encoded using the binary encoding method. The results, averaged over 50 independent runs, include error bars representing the standard deviation. The panels show the average obtainable fidelity as a function of optimization iteration for the following settings: (a) $\theta = -0.68\pi$ (dimerized), (b) $\theta = -0.55\pi$ (dimerized), (c) $\theta = -0.30\pi$ (dimerized), and (d) $\theta = -0.16\pi$ (Haldane).

ditionally, we see a notable performance drop as circuit depth increases beyond a certain point. This is due to the appearance of the Barren plateaus problem in the optimization landscape.

The VQE simulations with symmetry encoding utilize the total spin s preserving ansatz, as illustrated in Fig. 1(d). In this case, it is crucial to select an initial state that aligns with the symmetry preserving nature of the ansatz. Specifically, the ground state of the BBH model exhibits a total spin of $s=0$ across the dimerized, Haldane, and critical phases. Since the qubit Hamiltonian consists of $2N$ qubits, the initial state is taken to be $|\psi_0\rangle = \otimes^N |\psi^-\rangle$, where $|\psi^-\rangle = (|01\rangle - |10\rangle)/\sqrt{2}$. This initial state naturally has a total spin of $s=0$. As we will see, unlike the binary encoding, the symmetry encoding method can faithfully simulate the ground state in all phases. It is worth emphasizing that, the $|\psi^-\rangle$ is an illegitimate state for the qubits, however, as $|\psi_0\rangle = \otimes^N |\psi^-\rangle$ conserves the total spin it eventually reaches the true ground state.

Let's consider the BBH model with system size $N = 6$ at $\theta = -0.71\pi$ and $\theta = -0.3\pi$, both within the dimerized phase. In this region, the ground state of the qubit Hamiltonian represents the true ground state of the original system. Therefore, the illegitimate states do not influence the simulation outcomes. Consequently, the cost

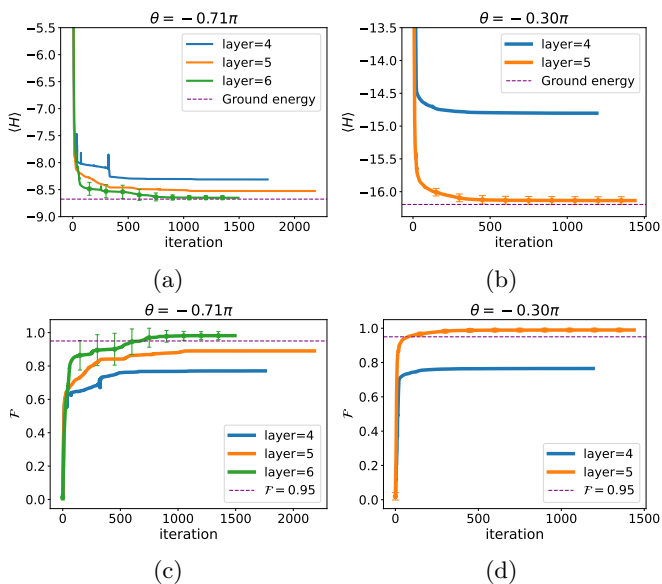


FIG. 4: The VQE simulation of the ground state of the spin-1 BBH model with system size $N=6$ for different values of θ in the dimerized phase. The corresponding qubit Hamiltonian uses 12 qubits, encoded using the symmetry encoding method. The results, averaged over 50 independent runs, include error bars representing the standard deviation. The upper panels (a)-(b) show the average energy as a function of optimization iteration for $\theta=-0.71\pi$ and $\theta=-0.30\pi$, respectively. The lower panels (c)-(d) show the corresponding average fidelity for $\theta=-0.71\pi$ and $\theta=-0.30\pi$.

function was simply defined as the expectation of the Hamiltonian, i.e. $\langle H \rangle$. The results of these VQE simulations are depicted in Figs. 4(a)-(d), where the average energy and obtainable fidelity are plotted as a function of optimization iterations for different ansatz layers. These results, whose error bars are computed over 50 independent runs, demonstrate that in both cases, the VQE simulations successfully converged to the ground state of the BBH model with a fidelity $\mathcal{F} \geq 0.95$ after ~ 1400 optimization iterations, employing 6 and 5 layers of the total spin-preserving ansatz, for $\theta = -0.71\pi$ and $\theta = -0.3\pi$ respectively.

Subsequently, we explore the Haldane phase of the BBH model, particularly at $\theta = -0.16\pi$ and $\theta = \arctan(1/3)$. Similar to the dimerized phase, in this phase also the ground state of the qubit Hamiltonian faithfully represents the true original Hamiltonian of the system. In other words, the illegitimate states become high-energy eigenstates. At the $\theta = \arctan(1/3)$ point, known as the Affleck-Kennedy-Lieb-Tasaki (AKLT) point, the ground state is four-fold degenerate, including a singlet state with total spin $s = 0$ and a triplet state with total spin $s = 1$. The AKLT point has a matrix product representation which makes its simulation accessible to classical computers. By using a total spin pre-

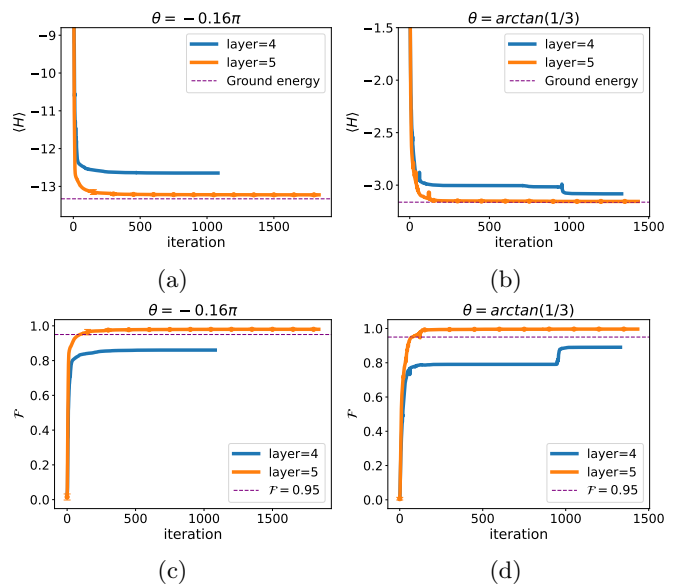


FIG. 5: The VQE simulation of the ground state of the spin-1 BBH model with system size $N=6$ for different values of θ in the Haldane phase. The corresponding qubit Hamiltonian uses 12 qubits, encoded using the symmetry encoding method. The results, averaged over 50 independent runs, include error bars representing the standard deviation. The upper panels (a)-(b) show the average energy as a function of optimization iteration for $\theta=-0.16\pi$ and $\theta = \arctan(1/3)$ (the AKLT point), respectively. The lower panels (c)-(d) show the corresponding average fidelity for $\theta=-0.16\pi$ and $\theta = \arctan(1/3)$.

serving ansatz, one can target any of these degenerate states by a proper choice of the initial state with a given total spin s . For instance, for simulating the ground state with total spin $s=0$ one can use the initial state $|\psi_0\rangle = \otimes^N |\psi^-\rangle$. On the other hand, for simulating the other ground states with $s=1$ one can replace one of the singlet states $|\psi^-\rangle$ by $|\psi^+\rangle = (|01\rangle + |10\rangle)/\sqrt{2}$ (for $s_z = 0$) or $|\phi^\pm\rangle = (|00\rangle \pm |11\rangle)/\sqrt{2}$ (for $s_z = \pm 1$). The VQE simulations with different numbers of ansatz layers are presented in Figs. 5(a)-(d). The error bars are computed for 50 different runs. Both simulations require 5 layers of the total spin-preserving ansatz to converge to the ground state of the BBH model with fidelity $\mathcal{F} \geq 0.95$. The convergence requires approximately 1750 and 1400 optimization iterations for $\theta = -0.16\pi$ and $\theta = \arctan(1/3)$, respectively. These results demonstrate the capability of the VQE algorithm to accurately simulate the Haldane phase.

We further explore the critical phase of the BBH model at $\theta = 0.32\pi$, a regime where illegitimate states significantly influence the simulation outcomes as they are becoming the low energy eigenstates of the system. In fact, for a system of $N = 6$, the real ground state of the original Hamiltonian corresponds to the eigenstate number

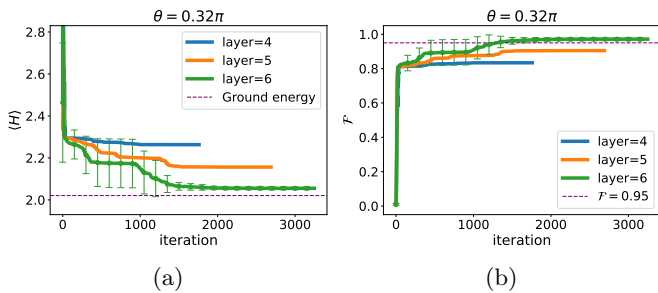


FIG. 6: The VQE simulation of the ground state of the spin-1 BBH model with system size $N=6$ for the critical phase. The corresponding qubit Hamiltonian uses 12 qubits, encoded using the symmetry encoding method. The results, averaged over 50 independent runs, include error bars representing the standard deviation. The average energy for $\theta=0.32\pi$, shown in panel (a), and the corresponding obtainable fidelity, shown in panel (b), is plotted as a function of optimization iteration.

1228 in the qubit Hamiltonian. In order to target the true ground state, we integrate a penalty term, as specified in Eqs. (21)–(22), into the VQE cost function with $\beta = 10$. The VQE results for various depths of the circuit, averaged over 50 independent trials, are depicted in Figs. 6(a)-(b). These results demonstrate that the simulations consistently converged to the ground state of the BBH model with a fidelity $\mathcal{F} \geq 0.95$ using a quantum circuit with 6 layers. Inevitably, the penalty term increases the computational cost of the VQE simulations, as indicated by the higher number of optimization iterations compared to other phases. Nonetheless, the simulations successfully capture the ground state of the BBH model in the critical phase, even though the true ground state of the original Hamiltonian is a high-energy eigenstate of the qubit Hamiltonian.

As discussed before, each phase of the BBH model is characterized by an order parameter. One can measure the order parameters at the output of the simulator. The results of these order parameters are presented in Fig. 7, which confirm that the VQE simulations accurately reproduce the ground state properties of the BBH model across the dimerized, Haldane, and critical phases.

B. VQE simulation of spin-3/2 models

For spin-1 systems, where both binary and symmetry encodings require the same number of qubits, the result for both cases shows a clear advantage on the symmetry encoding. This advantage is expected as exploiting symmetries in VQE simulations reduces the search subspace in the Hilbert subspace to only the relevant part in which all the states have the desired symmetries. This matches with the previous results for VQE simulation of qubit systems [97]. By increasing d , however, the binary and symmetry encoding methods require different numbers of

| Binary encoding, $N = 12$ | | | |
|-----------------------------|---------------------|---------------------|---------------------|
| | $\theta = -0.75\pi$ | $\theta = -0.36\pi$ | $\theta = -0.15\pi$ |
| #CNOT | 132 | 132 | 132 |
| #Para. | 312 | 312 | 312 |
| \mathcal{F} | 0.432 ± 0.417 | 0.806 ± 0.208 | 0.513 ± 0.256 |
| Iter. | 3076.4 ± 1082.7 | 2785.3 ± 1201.8 | 3244.2 ± 1211.9 |
| $C_R (\times 10^3)$ | 959.8 ± 337.8 | 869.0 ± 375.0 | 1012.2 ± 378.1 |
| Symmetry encoding, $N = 18$ | | | |
| | $\theta = -0.75\pi$ | $\theta = -0.36\pi$ | $\theta = -0.15\pi$ |
| #CNOT | 612 | 459 | 612 |
| #Para. | 204 | 153 | 204 |
| \mathcal{F} | 0.970 ± 0.008 | 0.951 ± 0.010 | 0.973 ± 0.011 |
| Iter. | 8806 ± 1839.7 | 4888.7 ± 1479.5 | 6958.2 ± 1712.9 |
| $C_R (\times 10^3)$ | 1796.4 ± 375.3 | 748.0 ± 226.4 | 1419.5 ± 350.4 |

TABLE I: Comparison between binary and symmetry encoding methods at (θ) for $N = 12$ and $N = 18$. The table shows the number of CNOT gates, the number of parameters, fidelity (\mathcal{F}), iteration count, and classical resources (C_R), with standard deviations for fidelity, iteration and classical resource metrics.

qubits. In this situation, it is not clear whether the symmetry encoding still performs better as it demands more qubits for the mapping. To explore this situation, we focus on a spin- $\frac{3}{2}$ model. We consider the same Hamiltonian as the spin-1 BBH model, shown in Eq. (23), but with the spin-1 operators replaced by spin- $\frac{3}{2}$ operators. The corresponding spin-3/2 operators are represented by matrices:

$$\begin{aligned} \tilde{S}^x &= \frac{1}{2} \begin{pmatrix} 0 & \sqrt{3} & 0 & 0 \\ \sqrt{3} & 0 & 2 & 0 \\ 0 & 2 & 0 & \sqrt{3} \\ 0 & 0 & \sqrt{3} & 0 \end{pmatrix}, \\ \tilde{S}^y &= \frac{1}{2i} \begin{pmatrix} 0 & \sqrt{3} & 0 & 0 \\ -\sqrt{3} & 0 & 2 & 0 \\ 0 & -2 & 0 & \sqrt{3} \\ 0 & 0 & -\sqrt{3} & 0 \end{pmatrix}, \\ \tilde{S}^z &= \frac{1}{2} \begin{pmatrix} 3 & 0 & 0 & 0 \\ 0 & 1 & 0 & 0 \\ 0 & 0 & -1 & 0 \\ 0 & 0 & 0 & -3 \end{pmatrix}. \end{aligned}$$

The spin-3/2 BBH model is a 4-level system with the basis determined by the eigenvalues of the S_z operator. The basis is then given by

$$\begin{aligned} |\tilde{0}\rangle &= |s_z = +\frac{3}{2}\rangle, & |\tilde{1}\rangle &= |s_z = +\frac{1}{2}\rangle, \\ |\tilde{2}\rangle &= |s_z = -\frac{1}{2}\rangle, & |\tilde{3}\rangle &= |s_z = -\frac{3}{2}\rangle. \end{aligned} \quad (28)$$

To encode these states into qubits using binary encoding one requires 2 qubits as:

$$\begin{aligned} |\tilde{0}\rangle &\mapsto |00\rangle, & |\tilde{1}\rangle &\mapsto |01\rangle, \\ |\tilde{2}\rangle &\mapsto |10\rangle, & |\tilde{3}\rangle &\mapsto |11\rangle. \end{aligned} \quad (29)$$

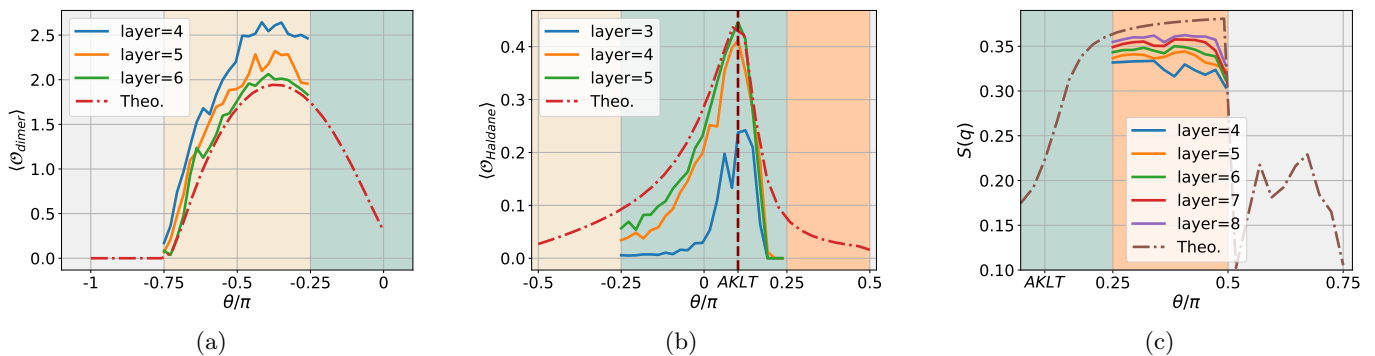


FIG. 7: The value of order parameters for the dimerized, Haldane, and critical phases of the BBH model, calculated using the output state of the VQE simulation, are shown in panels (a), (b), and (c), respectively. The results are averaged over 50 independent runs. As the number of total spin preserving ansatz layers increases, the obtained order parameters more closely align with the corresponding theoretical values.

On the other hand, the symmetry encoding method of the spin-3/2 BBH model, requires 3 qubits for each spin. The mapping for the symmetry encoding method is as follows:

$$\begin{aligned} |\tilde{0}\rangle &\mapsto |000\rangle, & |\tilde{1}\rangle &\mapsto \frac{1}{\sqrt{3}}(|001\rangle + |010\rangle + |100\rangle), \\ |\tilde{2}\rangle &\mapsto \frac{1}{\sqrt{3}}(|110\rangle + |101\rangle + |011\rangle), & |\tilde{3}\rangle &\mapsto |111\rangle. \end{aligned} \quad (30)$$

Thus, exploiting the symmetry in the spin-3/2 BBH model comes at the cost of using more qubits with the symmetry encoding method. Here, we compare the performance of binary encoding and symmetry encoding methods for VQE simulation of the spin-3/2 BBH model. In Table I, we present VQE simulation results for this model with $N = 6$ spins, which is mapped to qubit systems of size $2N$ and $3N$ for binary and symmetry encoding methods, respectively. The results are averaged over 50 independent runs. The table shows the number of CNOT gates (i.e. quantum resources), the number of parameters to optimize, obtainable fidelity, optimization iterations and classical resources, defined in Eq. (9), for three different values of θ . The results using binary encoding with a hardware-efficient ansatz are shown in the top half of the table, which fails to converge to fidelity $\mathcal{F} \geq 0.95$ for all values of θ . More importantly, adding more layers to the ansatz decreases the fidelity, indicating the presence of a Barren plateau problem in the VQE simulations. In contrast, the results using symmetry encoding with a total spin preserving ansatz, shown in the bottom half of the table, successfully converge to fidelity $\mathcal{F} \geq 0.95$ for all tested θ values. The results demonstrate that the symmetry encoding significantly outperforms the binary encoding despite the overhead of extra qubits. Note that these results are presented without implementing any Barren plateau mitigation techniques, which could potentially enhance both the performance of the binary and the symmetry encoding methods.

| | $U = -2$ | $U = 2$ |
|---------------------|----------------------|---------------------|
| #CNOT | 330 | 297 |
| #Para. | 230 | 207 |
| \mathcal{F} | 0.975 ± 0.004 | 0.999 ± 0.001 |
| Iter. | 11802.9 ± 2669.6 | 7538.8 ± 2183.5 |
| $C_R (\times 10^3)$ | 2714.7 ± 614.0 | 1560.5 ± 452.0 |

TABLE II: Simulation results for the Bose-Hubbard model with different interaction strengths (U). This table shows the number of CNOT gates, number of parameters, fidelity (\mathcal{F}), iteration count, and classical resources (C_R), with respective standard deviations, across two interaction strengths: $U = -2$, and $U = 2$.

C. VQE simulation of bosonic systems

Finally, we turn our attention to the simulation of bosonic systems in which $d \rightarrow \infty$. Specifically, we focus on the Bose-Hubbard model defined by the Hamiltonian:

$$\tilde{H}_{\text{BH}} = -t \sum_{i=1}^{N-1} (a_i^\dagger a_{i+1} + a_{i+1}^\dagger a_i) + \frac{U}{2} \sum n_i (n_i - 1), \quad (31)$$

where N is the size of the lattice, a_i^\dagger and a_i are the bosonic creation and annihilation operators at the i -th site, respectively, and $n_i = a_i^\dagger a_i$ is the number operator. The parameter t denotes the hopping strength, and U represents the on-site interaction. Note that the Bose-Hubbard Hamiltonian has a symmetry of preserving the total number of bosons as $[\tilde{H}_{\text{BH}}, \mathcal{W}] = 0$, where $\mathcal{W} = \sum_i n_i$ is the total number operator. Theoretically, the Bose-Hubbard model is infinite-dimensional, posing significant challenges for direct simulation on a qubit-based quantum simulator. However, by truncating the bosonic Hilbert space to a finite dimension, effective simulation becomes feasible. In fact, for a given number of bosons n_{bos} , namely $\langle \mathcal{W} \rangle = n_{\text{bos}}$, the Hilbert space of each site is naturally limited to $d = n_{\text{bos}} + 1$. Therefore, if the truncation number is below this value it may result in

some errors. Nonetheless, the truncation error may still be negligible in the limit of $U \gg 0$, where repulsive interaction between bosonic excitations makes the occupation number of each site as low as possible. In contrast, negative U , i.e. attractive interaction, tends to accumulate all the excitations on one site which naturally increases the Hilbert space of each site and thus enhances the truncation error. For our simulations, we adopt a truncation limit of four levels per site (i.e. $d=4$) represented by the bosonic Fock states $\{|\tilde{0}\rangle, |\tilde{1}\rangle, |\tilde{2}\rangle, |\tilde{3}\rangle\}$. Similar to the case of spin-3/2, the binary encoding with hardware efficient ansatz cannot converge to good results. Therefore, we only focus on the symmetry encoding approach. The encoding is as follows:

$$\begin{aligned} |\tilde{0}\rangle &\mapsto |000\rangle, \\ |\tilde{1}\rangle &\mapsto \frac{1}{\sqrt{3}}(|100\rangle + |010\rangle + |001\rangle), \\ |\tilde{2}\rangle &\mapsto \frac{1}{\sqrt{3}}(|110\rangle + |101\rangle + |011\rangle), \\ |\tilde{3}\rangle &\mapsto |111\rangle. \end{aligned} \quad (32)$$

Let's consider a lattice of $N=4$ sites which is mapped to a system of $3N$ qubits through $H_{\text{BH}} = \mathcal{T}_s \tilde{H}_{\text{BH}} \mathcal{T}_s^\dagger$. In other words, the 4-site Bose-Hubbard model is mapped to a 12-qubit system. We also assume that there are only $n_{\text{bos}}=3$ bosons in the systems. The symmetry encoding method effectively preserves the conservation of the total number of bosons. This conservation translates to the conservation of excitations in the qubit system, which also implies the conservation of z component of the total spin, denoted by $[H_{\text{BH}}, S_{\text{tot}}^z] = 0$. Thus, we utilize the s_z -conserving ansatz, as illustrated in Fig. 1(c).

Regarding the on-site interaction strength U , we investigate two distinct regimes, namely $U = \pm 2$. Ground state simulations with positive U values are relatively trivial as bosons naturally avoid clustering, resulting in the vacuum state as the ground state. Therefore, our simulations concentrate on the subspace with three bosons, i.e. $n_{\text{bos}}=3$, across four sites, i.e. $N=4$. The initial state of the VQE circuit is taken to be $|\psi_0\rangle = |\tilde{3}, \tilde{0}, \tilde{0}, \tilde{0}\rangle$ whose qubit representation is $|\psi_0\rangle = |111000000000\rangle$. With negative U , bosons tend to gather, challenging the limit of our truncated Hilbert space and complicating the VQE simulations. The results of these simulations are summarized in Table II, showing the resources required for the VQE to achieve a fidelity of $\mathcal{F} \geq 0.95$, averaged over 50 independent runs. The data clearly indicates that as U transitions from negative to positive, the computational demands for the VQE simulations decrease, implying easier simulation. These results show that the VQE simulations robustly converge to the ground state of the Bose-Hubbard model across all explored regimes, demonstrating the effectiveness of the VQE algorithm in accurately simulating bosonic systems.

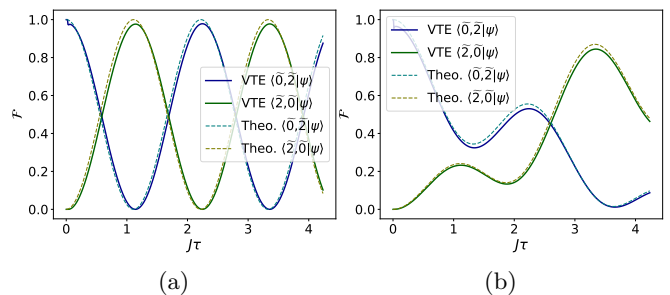


FIG. 8: The variational time evolution simulation of the spin-1 BBH model with system size $N=2$ over time $\tau=6/J$ for: (a) $\theta=\frac{\pi}{4}$, where $\frac{\cos(\theta)}{\sin(\theta)} = 1$; and (b)

$\theta=\arctan(\frac{1}{2})$, where $\frac{\cos(\theta)}{\sin(\theta)} = 0.5$. The corresponding qubit Hamiltonian uses 4 qubits, encoded using the symmetry encoding method. The average fidelity of the variational time evolution results states with two states $|\tilde{0}, \tilde{2}\rangle$, and $|\tilde{2}, \tilde{0}\rangle$ is plotted as a function of the evolution time, labeled VTE in the figure. The theoretical result of the time evolution of the system is shown in dash lines.

V. VARIATIONAL TIME EVOLUTION SIMULATION

In this section, we extend our study to include the variational time evolution of d -level systems using qubit-based quantum simulators. We specifically demonstrate the time evolution simulation of a spin-1 BBH model (i.e. $d=3$) shown in Eq. (23). Notably, this Hamiltonian conserves the z -component of the total spin, namely $([\tilde{H}_{\text{BBH}}, S_{\text{tot}}^z] = 0)$. Hence, for example, if the initial state of the system is chosen to be $|\tilde{0}, \tilde{2}\rangle$, as the time evolution proceeds, the state of the system can only be a superposition of states with the same total spin s_z , namely $|\tilde{0}, \tilde{2}\rangle$, $|\tilde{2}, \tilde{0}\rangle$, and $|\tilde{1}, \tilde{1}\rangle$. Furthermore, for the case of $\theta=\frac{\pi}{4}$, the Hamiltonian also conserve $\frac{1}{2} \sum_i (S_i^z)^2$. This implies that for $\theta = \pi/4$, the quantum state $|\tilde{0}, \tilde{2}\rangle$ remains in the subspace spanned by $|\tilde{0}, \tilde{2}\rangle$, and $|\tilde{2}, \tilde{0}\rangle$. In fact, the time evolution will act similar to a swap operation between the two states $|\tilde{0}, \tilde{2}\rangle$ and $|\tilde{2}, \tilde{0}\rangle$.

In order to perform variational time evolution, we consider a system of $N = 2$ spin-1 particles interacting under the BBH Hamiltonian with two different values of θ . Especially, $\theta = \pi/4$ ($\frac{\cos(\theta)}{\sin(\theta)} = 1$), where the time evolution acts similar to a state swapping process, and $\theta = \arctan(1/2)$ ($\frac{\cos(\theta)}{\sin(\theta)} = 0.5$), to demonstrate a typical non-equilibrium time evolution. We employ the symmetry encoding (19) to evolve the system up to time $\tau=6/J$, which requires 4 qubits. The initial state of the system is chosen to be $|\Psi(0)\rangle = |\tilde{0}, \tilde{2}\rangle$ which will be mapped to $|1100\rangle$ for the qubit simulation. The time evolution is given by $|\Psi(\tau)\rangle = \exp(-iH_{\text{BBH}}\tau)|\Psi(0)\rangle$. We utilize the total spin preserving ansatz, as illustrated in

Fig. 1(d). The variational time evolution simulation results are presented in Figs. 8(a)-(b), where two fidelities, namely $|\langle \hat{0}, \hat{2} | \Psi(\tau) \rangle|^2$ and $|\langle \hat{2}, \hat{0} | \Psi(\tau) \rangle|^2$, are plotted as a function of time $J\tau$. One can clearly see a good match between the exact results and the results from the variational time evolution. This demonstrates the capability of symmetry encoding in capturing the properties of the non-equilibrium dynamics of d -level systems through a variational time evolution algorithm.

VI. CONCLUSION

In this paper, we investigate variational quantum simulation of d -level systems on qubit-based quantum simulators. In particular, we consider higher spins and bosonic systems. Both ground state and non-equilibrium dynamics have been explored. We have compared two different types of encoding methods for such simulations, namely binary and symmetry encodings. While binary encoding is efficient with respect to the number of qubits, requiring only $\lceil \log_2(d) \rceil$ qubits per particle, it may not be able to incorporate the symmetries in the design of the quantum circuit. On the other hand, symmetry encoding requires $d-1$ qubits per particle to ensure preserving of typical symmetries, such as S_{tot}^2 and S_{tot}^z . In both of these methods, the Hilbert space of the qubit system is typically larger than the Hilbert space of the original d -

level system. This naturally introduces illegitimate states in the Hilbert space of the qubit system which has no correspondence in the real d -level system. By mapping the d -level Hamiltonian into qubit systems, sometimes the ground state of the qubit system lies in the illegitimate subspace. We have systematically introduced a penalty term which pushes the illegitimate states into high-energy states to guarantee the success of the VQE simulations. Interestingly, through simulation of a wide range of phases in spin-1, spin-3/2, as well as the Bose-Hubbard model, we observe that the binary encoding is not scalable as the hardware efficient ansatz cannot be trained due to the presence of Barren plateau. On the other hand, symmetry encoding, despite requiring extra qubits, does not face such trainability issue thanks to exploiting symmetries. Our proposal is very timely as it can be implemented on existing quantum simulators and can easily be generalized to cover a wide range of qudit models.

VII. ACKNOWLEDGEMENT

A.B. acknowledges support from the National Natural Science Foundation of China (Grants No. 12050410253, No. 92065115, and No. 12274059), and the Ministry of Science and Technology of China (Grant No. QNJ2021167001L)

-
- [1] J. Preskill, *Quantum* **2**, 79 (2018).
 - [2] R. P. Feynman, *International Journal of Theoretical Physics* **21**, 467 (1982).
 - [3] S. Lloyd, Quantum approximate optimization is computationally universal (2018), [arXiv:1812.11075](https://arxiv.org/abs/1812.11075) [quant-ph].
 - [4] P. Bordia, H. Lüschen, S. Scherg, *et al.*, *Phys. Rev. X* **7**, 041047 (2017).
 - [5] M. Schreiber, S. S. Hodgman, P. Bordia, *et al.*, *Science* **349**, 842 (2015).
 - [6] C. Gross and I. Bloch, *Science* **357**, 995 (2017).
 - [7] A. Omran, H. Levine, A. Keesling, *et al.*, *Science* **365**, 570 (2019).
 - [8] A. Keesling, A. Omran, H. Levine, *et al.*, *Nature* **568**, 207 (2019).
 - [9] J. Wang, S. Paesani, R. Santagati, *et al.*, *Nat. Phys.* **13**, 551 (2017).
 - [10] H.-S. Zhong, H. Wang, Y.-H. Deng, *et al.*, *Science* **370**, 1460 (2020).
 - [11] J. Carolan, M. Mohseni, J. P. Olson, *et al.*, *Nat. Phys.* **16**, 322 (2020).
 - [12] J. Li, R. Fan, H. Wang, *et al.*, *Phys. Rev. X* **7**, 031011 (2017).
 - [13] B. P. Lanyon, C. Hempel, D. Nigg, *et al.*, *Science* **334**, 57 (2011).
 - [14] J. Zhang, G. Pagano, P. W. Hess, *et al.*, *Nature* **551**, 601 (2017).
 - [15] C. Hempel, C. Maier, J. Romero, *et al.*, *Phys. Rev. X* **8**, 031022 (2018).
 - [16] C. Kokail, C. Maier, R. van Bijnen, *et al.*, *Nature* **569**, 355 (2019).
 - [17] Z. Han, C. Lyu, Y. Zhou, *et al.*, *Phys. Rev. Res.* **6**, 013015 (2024).
 - [18] Y. Salathé, M. Mondal, M. Oppliger, *et al.*, *Phys. Rev. X* **5**, 021027 (2015).
 - [19] C. S. Wang, J. C. Curtis, B. J. Lester, *et al.*, *Phys. Rev. X* **10**, 021060 (2020).
 - [20] A. H. Karamlou, W. A. Simon, A. Katarawa, *et al.*, *npj Quantum Inf.* **7**, 156 (2021).
 - [21] C. Neill, T. McCourt, X. Mi, *et al.*, *Nature* **594**, 508 (2021).
 - [22] J. Han, W. Cai, L. Hu, *et al.*, *Phys. Rev. Lett.* **127**, 020504 (2021).
 - [23] J. Braumüller, A. H. Karamlou, Y. Yanay, *et al.*, *Nat. Phys.* **18**, 172 (2022).
 - [24] X. Zhang, W. Jiang, J. Deng, *et al.*, *Nature* **607**, 468–473 (2022).
 - [25] Y.-H. Shi, Y. Liu, Y.-R. Zhang, *et al.*, *Phys. Rev. Lett.* **131**, 080401 (2023).
 - [26] M. H. Levitt, *Spin dynamics: basics of nuclear magnetic resonance* (John Wiley & Sons, 2013).
 - [27] M. P. A. Fisher, P. B. Weichman, G. Grinstein, and D. S. Fisher, *Phys. Rev. B* **40**, 546 (1989).
 - [28] E. B. Wilson, J. C. Decius, P. C. Cross, and B. R. Sundheim, *J. Electrochem. Soc.* **102**, 235Ca (1955).
 - [29] M. Shimizu, *Rep. Prog. Phys.* **44**, 329 (1981).
 - [30] A. Glos, A. Krawiec, and Z. Zimborás, *npj Quantum Inf.* **8**, 39 (2022).

- [31] Z. Tabi, K. H. El-Safty, Z. Kallus, *et al.*, in *2020 IEEE International Conference on Quantum Computing and Engineering (QCE)* (2020) pp. 56–62.
- [32] P. Liu, R. Wang, J.-N. Zhang, *et al.*, *Phys. Rev. X* **13**, 021028 (2023).
- [33] M. Meth, J. F. Haase, J. Zhang, *et al.*, Simulating 2d lattice gauge theories on a qudit quantum computer (2024), [arXiv:2310.12110 \[quant-ph\]](#).
- [34] T. V. Zache, D. González-Cuadra, and P. Zoller, *Quantum* **7**, 1140 (2023).
- [35] D. González-Cuadra, T. V. Zache, J. Carrasco, *et al.*, *Phys. Rev. Lett.* **129**, 160501 (2022).
- [36] P. Hrmo, B. Wilhelm, L. Gerster, *et al.*, *Nat. Commun.* **14**, 2242 (2023).
- [37] M. Ringbauer, M. Meth, L. Postler, *et al.*, *Nat. Phys.* **18**, 1053 (2022).
- [38] M. Luo and X. Wang, *Sci. China Phys. Mech. Astron.* **57**, 1712 (2014).
- [39] M. Meth, J. F. Haase, J. Zhang, *et al.*, [arXiv:2310.12110 \(2023\)](#).
- [40] D. González-Cuadra, T. V. Zache, J. Carrasco, *et al.*, *Physical Review Letters* **129**, 160501 (2022).
- [41] L.-A. Wu and D. A. Lidar, *J. Math. Phys.* **43**, 4506 (2002).
- [42] C. D. Batista and G. Ortiz, *Adv. Phys.* **53**, 1 (2004).
- [43] N. P. D. Sawaya, T. Menke, T. H. Kyaw, *et al.*, *npj Quantum Inf.* **6**, 49 (2020).
- [44] R. H. Dicke, *Phys. Rev.* **93**, 99 (1954).
- [45] K. Yang, Y. Zhu, X. Zeng, *et al.*, Cost of locally approximating high-dimensional ground states of contextual quantum models (2024), [arXiv:2405.04884 \[quant-ph\]](#).
- [46] H.-S. Zhong, Y.-H. Deng, J. Qin, *et al.*, *Phys. Rev. Lett.* **127**, 180502 (2021).
- [47] Y.-H. Deng, Y.-C. Gu, H.-L. Liu, *et al.*, *Phys. Rev. Lett.* **131**, 150601 (2023).
- [48] F. Arute, K. Arya, R. Babbush, *et al.*, *Science* **369**, 1084–1089 (2020).
- [49] P. J. J. O’Malley, R. Babbush, I. D. Kivlichan, *et al.*, *Phys. Rev. X* **6**, 031007 (2016).
- [50] A. Kandala, A. Mezzacapo, K. Temme, *et al.*, *Nature* **549**, 242 (2017).
- [51] J. I. Colless, V. V. Ramasesh, D. Dahlen, *et al.*, *Phys. Rev. X* **8**, 011021 (2018).
- [52] Y. Nam, J.-S. Chen, N. C. Panti, *et al.*, *npj Quantum Inf.* **6**, 33 (2020).
- [53] E. Farhi, J. Goldstone, and S. Gutmann, A quantum approximate optimization algorithm (2014), [arXiv:1411.4028 \[quant-ph\]](#).
- [54] S. Bravyi, A. Kliesch, R. Koenig, and E. Tang, *Phys. Rev. Lett.* **125**, 260505 (2020).
- [55] M. Karácsony, L. Oroszlány, and Z. Zimboras, *SciPost Phys. Core* **7**, 032 (2024).
- [56] J. Biamonte, P. Wittek, N. Pancotti, *et al.*, *Nature* **549**, 195 (2017).
- [57] S. Arunachalam and R. de Wolf, A survey of quantum learning theory (2017), [arXiv:1701.06806 \[quant-ph\]](#).
- [58] C. Ciliberto, M. Herbster, A. D. Ialongo, *et al.*, *Proc. R. Soc. A: Math. Phys. Eng. Sci.* **474**, 20170551 (2018).
- [59] V. Dunjko and H. J. Briegel, *Reports on Progress in Physics* **81**, 074001 (2018).
- [60] E. Farhi and H. Neven, Classification with quantum neural networks on near term processors (2018), [arXiv:1802.06002 \[quant-ph\]](#).
- [61] M. Schuld and N. Killoran, *Phys. Rev. Lett.* **122**, 040504 (2019).
- [62] S. A. Wilkinson and M. J. Hartmann, Evaluating the performance of sigmoid quantum perceptrons in quantum neural networks (2022), [arXiv:2208.06198 \[quant-ph\]](#).
- [63] P. Zapletal, N. A. McMahon, and M. J. Hartmann, Error-tolerant quantum convolutional neural networks for symmetry-protected topological phases (2023), [arXiv:2307.03711 \[quant-ph\]](#).
- [64] C. Cirstoiu, Z. Holmes, J. Iosue, *et al.*, *npj Quantum Inf.* **6**, 1 (2020).
- [65] J. Gibbs, K. Gili, Z. Holmes, *et al.*, Long-time simulations with high fidelity on quantum hardware (2021), [arXiv:2102.04313 \[quant-ph\]](#).
- [66] X. Yuan, S. Endo, Q. Zhao, *et al.*, *Quantum* **3**, 191 (2019).
- [67] S. McArdle, T. Jones, S. Endo, *et al.*, *npj Quantum Inf.* **5**, 1 (2019).
- [68] K. Heya, K. M. Nakanishi, K. Mitarai, *et al.*, Subspace variational quantum simulator (2023), [arXiv:1904.08566 \[quant-ph\]](#).
- [69] J. Huh, S. Mostame, T. Fujita, *et al.*, *New J. Phys.* **16**, 123008 (2014).
- [70] Z. Hu, R. Xia, and S. Kais, *Sci. Rep.* **10**, 1 (2020).
- [71] S. Endo, J. Sun, Y. Li, *et al.*, *Phys. Rev. Lett.* **125**, 010501 (2020).
- [72] T. Haug and K. Bharti, *Quantum Sci. Technol.* **7**, 045019 (2022).
- [73] J. J. Meyer, J. Borregaard, and J. Eisert, *npj Quantum Inf.* **7**, 1 (2021).
- [74] J. J. Meyer, *Quantum* **5**, 539 (2021).
- [75] J. L. Beckey, M. Cerezo, A. Sone, and P. J. Coles, *Phys. Rev. Res.* **4**, 013083 (2022).
- [76] R. Kaubruegger, P. Silvi, C. Kokail, *et al.*, *Phys. Rev. Lett.* **123**, 260505 (2019).
- [77] B. Koczor, S. Endo, T. Jones, *et al.*, *New J. Phys.* **22**, 083038 (2020).
- [78] Z. Ma, P. Gokhale, T.-X. Zheng, *et al.*, in *2021 IEEE International Conference on Quantum Computing and Engineering (QCE)* (IEEE, 2021).
- [79] T. Haug and M. S. Kim, *Phys. Rev. A* **106**, 052611 (2022).
- [80] R. Sagastizabal, S. P. Premaratne, B. A. Klaver, *et al.*, *npj Quantum Inf.* **7**, 130 (2021).
- [81] C. Lyu, V. Montenegro, and A. Bayat, *Quantum* **4**, 324 (2020).
- [82] K. M. Nakanishi, K. Mitarai, and K. Fujii, *Phys. Rev. Res.* **1**, 033062 (2019).
- [83] O. Higgott, D. Wang, and S. Brierley, *Quantum* **3**, 156 (2019).
- [84] J. R. McClean, M. E. Kimchi-Schwartz, J. Carter, and W. A. De Jong, *Phys. Rev. A* **95**, 042308 (2017).
- [85] R. Santagati, J. Wang, A. A. Gentile, *et al.*, *Sci. Adv.* **4**, eaap9646 (2018).
- [86] C.-L. Hong, L. Colmenarez, L. Ding, *et al.*, Quantum parallelized variational quantum eigensolvers for excited states (2023), [arXiv:2306.11844 \[quant-ph\]](#).
- [87] V. Feulner and M. J. Hartmann, *Phys. Rev. B* **106**, 144426 (2022).
- [88] P. K. Barkoutsos, J. F. Gonthier, I. Sokolov, *et al.*, *Phys. Rev. A* **98**, 022322 (2018).
- [89] H. Wang, S. Ashhab, and F. Nori, *Phys. Rev. A* **79**, 042335 (2009).

- [90] K. Seki, T. Shirakawa, and S. Yunoki, *Phys. Rev. A* **101**, 052340 (2020).
- [91] B. T. Gard, L. Zhu, G. S. Barron, *et al.*, *npj Quantum Inf.* **6**, 10 (2020).
- [92] G. S. Barron, B. T. Gard, O. J. Altman, *et al.*, *Phys. Rev. Appl.* **16**, 034003 (2021).
- [93] F. Zhang, N. Gomes, N. F. Berthussen, *et al.*, *Phys. Rev. Res.* **3**, 013039 (2021).
- [94] H. Zheng, Z. Li, J. Liu, *et al.*, *PRX Quantum* **4**, 020327 (2023).
- [95] J. R. McClean, J. Romero, R. Babbush, and A. Aspuru-Guzik, *New J. Phys.* **18**, 023023 (2016).
- [96] I. G. Ryabinkin, S. N. Genin, and A. F. Izmaylov, *J. Chem. Theory Comput.* **15**, 249 (2018).
- [97] C. Lyu, X. Xu, M.-H. Yung, and A. Bayat, *Quantum* **7**, 899 (2023).
- [98] R. Wiersema, C. Zhou, Y. de Sereville, *et al.*, *PRX Quantum* **1**, 020319 (2020).
- [99] J. Haegeman, B. Pirvu, D. J. Weir, *et al.*, *Phys. Rev. B* **85**, 100408 (2012).
- [100] F. Vicentini, A. Biella, N. Regnault, and C. Ciuti, *Phys. Rev. Lett.* **122**, 250503 (2019).
- [101] Y. Huang, Q. Li, X. Hou, *et al.*, *Phys. Rev. A* **105**, 052414 (2022).
- [102] D. C. Liu and J. Nocedal, *Math. Program.* **45**, 503 (1989).
- [103] Y. Li and S. C. Benjamin, *Phys. Rev. X* **7**, 021050 (2017).
- [104] J. R. McClean, S. Boixo, V. N. Smelyanskiy, *et al.*, *Nat. Commun.* **9**, 4812 (2018).
- [105] Z. Holmes, K. Sharma, M. Cerezo, and P. J. Coles, *PRX Quantum* **3**, 010313 (2022).
- [106] F. Vatan and C. Williams, *Phys. Rev. A* **69**, 032315 (2004).
- [107] G. De Chiara, M. Lewenstein, and A. Sanpera, *Phys. Rev. B* **84**, 054451 (2011).

Appendix A: Qubit Hamiltonian of Spin-1 BBH model with Binary Encoding

Here, we provide the exact form of result obtained by applying the binary encoding method to the spin-1 Bilinear-Biquadratic Heisenberg (BBH) Hamiltonian, as

shown in Eqs. (13)-(14). The qubit Hamiltonian for the spin-1 BBH model, after implementing the transformation described in Eq. (15), is as follows:

$$\begin{aligned} \tilde{S}_i \cdot \tilde{S}_{i+1} \mapsto & \frac{1}{8} (\sigma_{j+1}^x \sigma_{j+3}^x + \sigma_{j+1}^x \sigma_{j+2}^z \sigma_{j+3}^x + \sigma_{j+1}^x \sigma_{j+2}^x \\ & - \sigma_{j+1}^x \sigma_{j+2}^x \sigma_{j+3}^z + \sigma_j^z \sigma_{j+1}^x \sigma_{j+3}^x + \sigma_j^z \sigma_{j+1}^x \sigma_{j+2}^z \sigma_{j+3}^x \\ & + \sigma_j^z \sigma_{j+1}^x \sigma_{j+2}^x - \sigma_j^z \sigma_{j+1}^x \sigma_{j+2}^z \sigma_{j+3}^x + \sigma_j^x \sigma_{j+3}^x \\ & + \sigma_j^x \sigma_{j+2}^z \sigma_{j+3}^x + \sigma_j^x \sigma_{j+2}^x - \sigma_j^x \sigma_{j+2}^z \sigma_{j+3}^x \\ & - \sigma_j^x \sigma_{j+1}^x \sigma_{j+3}^z - \sigma_j^x \sigma_{j+1}^z \sigma_{j+2}^z \sigma_{j+3}^x - \sigma_j^x \sigma_{j+1}^x \sigma_{j+2}^x \\ & + \sigma_j^x \sigma_{j+1}^z \sigma_{j+2}^z \sigma_{j+3}^x + \sigma_{j+1}^y \sigma_{j+3}^x + \sigma_{j+1}^y \sigma_{j+2}^z \sigma_{j+3}^x \\ & + \sigma_{j+1}^y \sigma_{j+2}^y - \sigma_{j+1}^y \sigma_{j+2}^z \sigma_{j+3}^z + \sigma_j^z \sigma_{j+1}^y \sigma_{j+3}^x \\ & + \sigma_j^z \sigma_{j+1}^y \sigma_{j+2}^z \sigma_{j+3}^x + \sigma_j^z \sigma_{j+1}^y \sigma_{j+2}^y - \sigma_j^z \sigma_{j+1}^y \sigma_{j+2}^z \sigma_{j+3}^z \\ & + \sigma_j^y \sigma_{j+3}^x + \sigma_j^y \sigma_{j+2}^z \sigma_{j+3}^x + \sigma_j^y \sigma_{j+2}^y - \sigma_j^y \sigma_{j+2}^z \sigma_{j+3}^z \\ & - \sigma_j^y \sigma_{j+1}^z \sigma_{j+3}^y - \sigma_j^y \sigma_{j+1}^z \sigma_{j+2}^z \sigma_{j+3}^y - \sigma_j^y \sigma_{j+1}^z \sigma_{j+2}^y \\ & + \sigma_j^y \sigma_{j+1}^z \sigma_{j+2}^z \sigma_{j+3}^z) + \frac{1}{4} (\sigma_j^z \sigma_{j+2}^z + \sigma_j^z \sigma_{j+3}^z \\ & + \sigma_{j+1}^z \sigma_{j+2}^z + \sigma_{j+1}^z \sigma_{j+3}^z) \end{aligned} \quad (\text{A1})$$

$$\begin{aligned} (\tilde{S}_i \cdot \tilde{S}_{i+1})^2 \mapsto & \frac{3}{4} I + \frac{1}{4} (\sigma_{j+2}^z + \sigma_j^z - \sigma_{j+3}^z - \sigma_j^z \sigma_{j+3}^z \\ & - \sigma_{j+1}^z \sigma_{j+2}^z - \sigma_{j+1}^z) + \frac{1}{8} (\sigma_j^x \sigma_{j+1}^x \sigma_{j+2}^x \sigma_{j+3}^x + \sigma_j^y \sigma_{j+1}^x \sigma_{j+2}^y \sigma_{j+3}^x \\ & - \sigma_j^x \sigma_{j+1}^x \sigma_{j+2}^y \sigma_{j+3}^y + \sigma_j^y \sigma_{j+1}^x \sigma_{j+2}^x \sigma_{j+3}^y + \sigma_j^z \sigma_{j+1}^x \sigma_{j+2}^x \sigma_{j+3}^z \\ & + \sigma_j^x \sigma_{j+1}^y \sigma_{j+2}^x \sigma_{j+3}^x + \sigma_j^y \sigma_{j+1}^y \sigma_{j+2}^y \sigma_{j+3}^x + \sigma_j^x \sigma_{j+1}^y \sigma_{j+2}^x \sigma_{j+3}^y \\ & + \sigma_{j+1}^x \sigma_{j+2}^z \sigma_{j+3}^z - \sigma_j^z \sigma_{j+1}^y \sigma_{j+2}^y - \sigma_{j+1}^x \sigma_{j+2}^x + \sigma_j^z \sigma_{j+1}^y \sigma_{j+2}^z \sigma_{j+3}^z \\ & - \sigma_j^y \sigma_{j+3}^y + \sigma_j^x \sigma_{j+1}^z \sigma_{j+2}^z \sigma_{j+3}^x - \sigma_j^y \sigma_{j+2}^z \sigma_{j+3}^y + \sigma_j^x \sigma_{j+1}^z \sigma_{j+3}^x \\ & + \sigma_j^y \sigma_{j+1}^z \sigma_{j+3}^y - \sigma_j^x \sigma_{j+2}^z \sigma_{j+3}^x + \sigma_j^y \sigma_{j+1}^z \sigma_{j+2}^z \sigma_{j+3}^y \\ & - \sigma_j^x \sigma_{j+3}^x) + \frac{1}{4} (\sigma_{j+2}^z \sigma_{j+3}^z + \sigma_j^z \sigma_{j+1}^z + \sigma_j^z \sigma_{j+1}^z \sigma_{j+2}^z \sigma_{j+3}^z) \end{aligned} \quad (\text{A2})$$